Nanomaterials

DOI: 10.1002/anie.201102489

Rational Design of Functional Oxide Thin Films with Embedded Magnetic or Plasmonic Metallic Nanoparticles**

Naoufal Bahlawane, Katharina Kohse-Höinghaus, Thomas Weimann, Peter Hinze, Sarah Röhe, and Marcus Bäumer*

Extensive efforts are devoted to the development of metal nanostructures for applications with far-reaching technological impacts. Compelling examples include the enhancement of photocatalysis[1–4] and photoluminescence.[5,6] Thus, silver nanoparticles provide significant enhancement of the photocatalytic performance of TiO_2,[2] and of the photoluminescence of InGaN/GaN quantum wells.[6] Also, magnetoelectric nanocomposites were proposed for the fabrication of devices with magnetically controlled piezoelectricity[7] and high-density magnetic data storage.[8] The synthesis of functional oxide thin films with embedded metallic nanoparticles can be achieved by several approaches, as recently reviewed by Walters and Parkin.[9] The reported processes rely on sol–gel,[1,10,11] physical,[12] and chemical[13,14] vapor deposition (CVD). The functionality of the metal–metal-oxide nanocomposite thin films strongly depends on architectural characteristics, such as the size and density of the metallic nanoparticles, and on the composition of both phases. Beside achievements with gold-based nanocomposites, none of the proposed processes has achieved a reliable and individual control of all these characteristics.

To reach this objective, which is a prerequisite for the systematic design of nanocomposite functionality, we demonstrate herein the potential of a new approach that relies on mild and selective chemistries involving a weak oxidant and a selective reducer. We have recently reported the growth of technologically relevant magnetic and plasmonic metals and alloys, including Fe, Co, Ni, Cu, Ag, Pt, and Ru, by an approach that is driven by the intrinsic catalytic reactivity of the corresponding metal cations used as precursors (β-

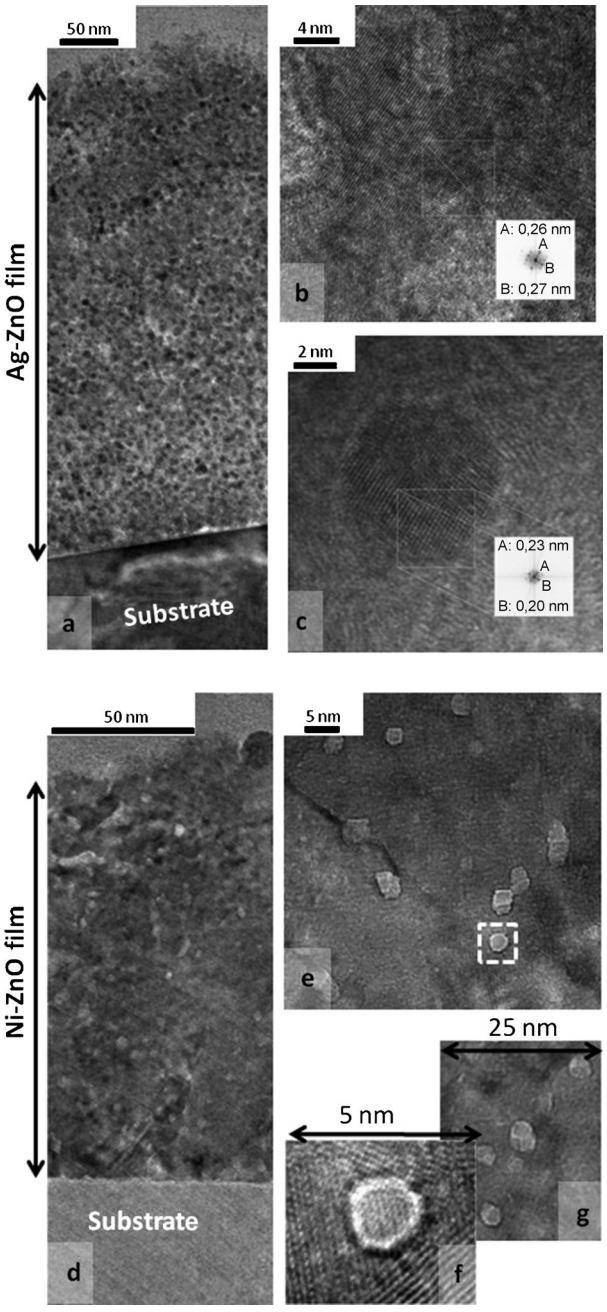

Figure 1. TEM views of the as-grown Ag-ZnO (a–c) and Ni-ZnO (d–g) nanocomposite thin film. Views of the cross-section of the layers are given in (a) and (d); b) ZnO matrix area in the Ag-ZnO nanocomposite; c) an individual Ag nanoparticle in the ZnO matrix, while (e–g) show nickel nanoparticles in the ZnO oxide matrix.

[*] Dr. N. Bahlawane,[+] Prof. Dr. K. Kohse-Höinghaus
Department of Chemistry, Bielefeld University
Universitaetsstrasse 25, 33615 Bielefeld (Germany)
E-mail: naoufal.bahlawane@uni-bielefeld.de
Dr. T. Weimann, Dipl.-Eng. P. Hinze
G 2.44—Nanostructures for Technical Applications
Physikalisch-Technische Bundesanstalt Braunschweig and Berlin
Bundesallee 100, 38116 Braunschweig (Germany)
Dipl.-Chem. S. Röhe, Prof. Dr. M. Bäumer
Institute of Applied and Physical Chemistry
Bremen University, 28334 Bremen (Germany)
[+] Current address: Nanomaterials Research Unit, SAM Department
Centre de Recherche Public—Gabriel Lippmann
41, rue du Brill, 4422 Belvaux (Luxembourg)
E-mail: bahlawan@lippmann.lu

[**] We acknowledge the financial support of the German Research Foundation (DFG, project number BA 2307/3-1 and BA 1710/20-1).
Supporting information for this article is available on the WWW under http://dx.doi.org/10.1002/anie.201102489.

diketonate complexes in general).[15,16] Cations of these metals, thereafter referred to as M1 category, are efficient redox catalysts and we have shown using in-situ mass spectrometry their ability to convert primary alcohols into aldehydes, driving their own reduction under CVD conditions. The catalytic dehydrogenation of primary alcohols occurs above 190 °C and makes hydrogen atoms locally available for the stabilization of the diketonate ligands of the metal precursor, which evaporate resulting in device-quality metallic thin films. The overall reaction is highly selective and non-sensitive to the presence of small fractions of weak oxidizers, such as water vapor. Interestingly, metals which do not exhibit enhanced thermally activated redox catalytic reactivity are insensitive to the presence of primary alcohols and therefore they are able to react with water vapor to form the corresponding oxides. This category of metals is referred to as M2 and includes Zn, Sn, and Ti, the oxide phases of which exhibit interesting opto-electro-chemical properties. Therefore, the growth of nanocomposite thin films formed by embedded M1 metallic nanoparticles in a M2 oxide matrix can be performed by CVD using alcohol as a selective reducer and water as a weak oxidizer. This single-pot process is described in the Supporting Information. Evidence is provided below regarding the growth of nanocomposites containing nanoparticles of noble and reactive metals, and an example is given which demonstrates the systematic tuning of the plasmonic properties of Au-ZnO-based nanocomposites by the adjustment of the particle size/density and composition of both phases.

Ag-ZnO and Ni-ZnO nanocomposite thin films were grown using the M1/M2 oxide strategy, with TEM cross-sectional micrographs presented in Figure 1 a–c and Figure 1 d–g. These films were obtained by alternating tailored pulse sequences of $t_{oxide} = 20$ min for the deposition of the oxide phase and $t_{metal} = 2$ min for the deposition of the metallic nanoparticles. The presence of two phases forming a dense film can be distinguished in both cases. The micrographs in Figures 1 a and 1 d show that nanocomposite films with homogeneously distributed nanoparticles can be grown to reach thicknesses of several hundred nanometers. The in-situ formation of the metallic nanoparticles, prevents their agglomeration and migration to the surface in contrast to what is found in sol–gel and CVD processes with preformed metallic nanoparticles.[10,11,14]

The high-resolution TEM micrograph of the Ag-ZnO nanocomposite in the matrix area (Figure 1 b) shows characteristic interplanar spacing of the ZnO hexagonal lattice [A: (002); B: (100)/PDF#36-1451], whereas the nanoparticles (Figure 1 c) are faceted, single crystalline, and have the interplanar spacing of the cubic lattice of metallic silver [A: (111); B: (200)/PDF#04-0783]. Figure 1 c shows a close contact at the nanoparticle–matrix interface. The mean crystallite size of 9.7 nm calculated from the X-ray diffraction (XRD) patterns is slightly larger than the size of 5–7 nm determined by TEM, which is probably due to the presence of a small fraction of larger particles.

The metallic nanoparticles in the Ni-ZnO nanocomposite, Figure 1 e–g, are also faceted and at 2–4 nm, slightly smaller than the silver nanoparticles. The metallic nature of the embedded nanoparticles was confirmed in the X-ray photoemission spectroscopy (XPS) analysis (Figure 2) by the absence of multiplets and shake-up-related satellites that

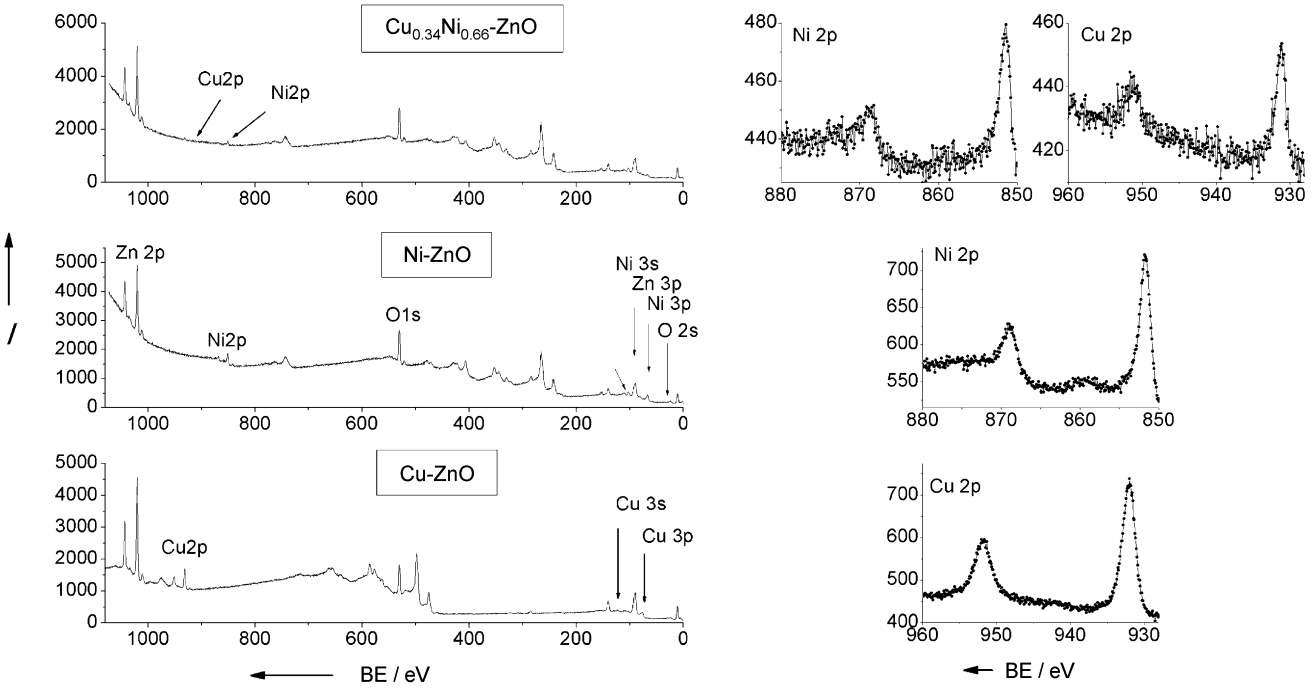

Figure 2. XPS wide scans of the Ni-ZnO, Cu-ZnO, and $Cu_{0.34}Ni_{0.66}$-ZnO nanocomposite thin films, and high-resolution Ni 2p and Cu 2p peaks. For clarity, only selected XPS peaks were assigned, the non-assigned peaks correspond to Auger and minor XPS lines of Zn, O, Ni, or Cu. It is worth noting that the X-ray source for the analysis of Ni-ZnO and CuNi-ZnO differs from that used for the analysis of the Cu-ZnO to minimize the Auger peaks overlapping. The bulk composition of the films was obtained after Ar-ion etching of the surface. (BE: binding energy.)

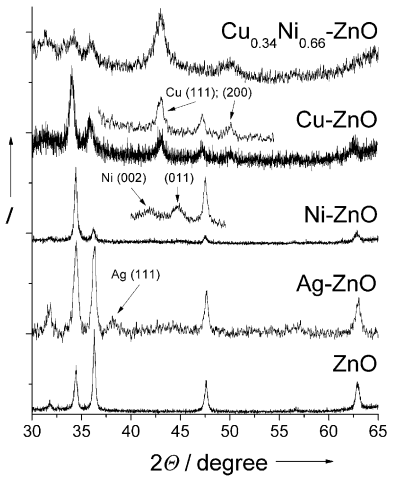

Figure 3. XRD patterns of the as-grown Ni-ZnO and Cu-ZnO nanocomposite thin films and the pattern of a ZnO thin film. Zinc oxide diffractogram fits to the reference spectrum PDF no. 36-1451 of the hexagonal lattice with the group symmetry (SG) P63 mc. The observed reflexes correspond to (100), (002), (101), (102), and (103) from left to right. Embedded silver in Ag-ZnO nanocomposite exhibits a characteristic reflex of the cubic lattice (PDF no. 04-0783, SG: *Fm3m*), nickel in Ni-ZnO exhibits characteristic reflexes of the hexagonal structure PDF no. 45-1027 with the SG: *P63/mmc*, while Cu in Cu-ZnO corresponds to the cubic lattice PDF no. 04-0836 with the SG: *Fm3m*.

characterize oxidized nickel. The XRD analysis in Figure 3 indicates that nickel nanoparticles embedded in ZnO crystallize in the hexagonal lattice (hcp). Previous studies shows that nickel deposition from $Ni(acac)_2$ and ethanol yields the hcp structure at low temperature while the cubic structure is grown at 290 °C or more.[15,17] TEM also indicates some hexagonal faceted nanoparticles with (Figure 1 g). The mean crystallite size of nickel nanoparticles was calculated to be 4.4 nm from the diffraction peaks broadening, in agreement with the TEM observations. Combining the film's composition extracted from XPS analysis and the particle sizes from XRD, the density of particles in the film was estimated to be 1.9×10^{18} particles cm^{-3}. Composites containing metallic nickel nanoparticles can be considered as a basis for the development of 3D high-density magnetic recording media, and the association with ZnO is likely to result in magnetoelectric behavior. The magnetism of the nanoparticles can be adjusted by alloying, whereas their size and density in the matrix can be adjusted by controlling t_{metal} and t_{oxide} successively.

Figure 2 and Figure 3 also show the results of XPS and XRD analyses of as-grown Cu-ZnO thin films using the same deposition conditions. They confirm clearly the metallic nature of the embedded copper nanoparticles with a mean crystallite size of 11.6 nm and a density of 7×10^{16} nanoparticles cm^{-3}.

The process can be extended to the incorporation of alloy nanoparticles by simply utilizing an alcohol cocktail of the targeted metals with the desired ratio. The XPS and XRD analyses of $Cu_{0.34}Ni_{0.66}$-ZnO nanocomposite thin film are presented in Figure 2 and Figure 3. Both elements, Cu and Ni, are present in the metallic state forming one alloy crystalline phase with a mean crystallite size of 6.6 nm and a density of 2.2×10^{17} nanoparticles cm^{-3}. The results in Figures 1–3 demonstrate the versatility of the catalytically driven CVD as a tool for the controlled synthesis of metal oxide matrices with embedded reactive or noble metal nanoparticles and their alloys.

Metallic nanoparticles show a strong optical absorption in the visible spectral range due to the localized surface plasmon (SP) resonance, which is a collective oscillation of the conduction electrons that is described by the Mie theory.[18] It is accepted that surface plasmons can excite semiconductors and semiconductors can excite surface plasmons.[4] As a result of this energy transfer, SPs can increase the density of states and the spontaneous emission rate in the semiconductor, leading to an enhancement of light emission in, for example, light-emitting diodes (LEDs),[6] SPs can also focus and trap light in thin films, which is useful for the improvement of the efficiency of photovoltaic devices.[19] Coupling of spontaneous emission or light absorption from the semiconductor material into the SPs of the metallic nanoparticles requires short distances since the SP is, in nature, an evanescent wave that exponentially decays with the distance.[6] This criterion is best achieved when the metallic nanoparticles are embedded into the functional semiconductor. A second requirement is the occurrence of resonant energy transfer, which is achieved when the oscillator frequencies of SP and semiconductor overlap. Several parameters might be controlled to adjust the SP resonance frequency, and the CVD process described herein is very suitable for fine-tuning these parameters.

Au-ZnO nanocomposite films were deposited with increased t_{metal}. The recorded spectra show a linear red shift of the surface plasmon resonance (SPR) from 478 nm with $t_{metal}=2$ min 30 s to 570 nm with $t_{metal}=45$ min as shown in Figure 4(1a,1b). The size of Au nanoparticles increases linearly with t_{metal} to reach 25 nm at $t_{metal}=60$ min. This change in the particle size is insufficient to explain the large effect on the SPR frequency. It is however worth mentioning that the spill-out effect dominates for sub-10 nm Au-particles[20] and is expected to blue-shift the SPR frequency at short t_{metal}; while the plasmon coupling effect for close-lying Au particles[21] induces a red-shift at long t_{metal}. These two effects add to the particle size effect to enable the plasmon frequency tuning in a wide spectral range. As a metallic overlayer[22] or in solution,[23] a linear trend of the SPR band maximum with the particle size was also observed, but no systematic study was reported for embedded metal particles in thin film matrices.

An independent parameter for the control of the SPR frequency, in addition to the variation of the dielectric function of the metallic nanoparticles (see Supporting Information), is the alteration of the refractive index of the host oxide matrix, which can be increased in ZnO by titanium doping. According to Mie's theory, the SPR band maximum depends on the medium's refractive index (n), as described by Equation (1), where m_e and e are the electron's mass and charge, ε_0 is the high-frequency dielectric constant of the metal, and N_e is the density of free electrons on the metal nanoparticles.[24]

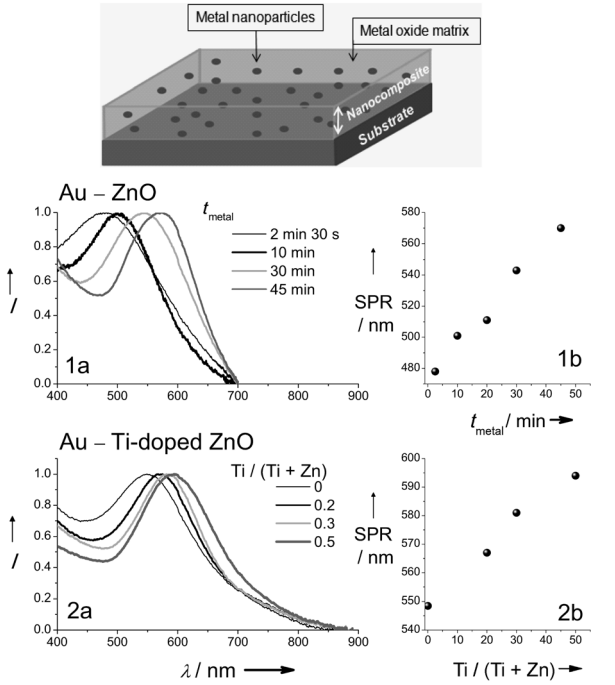

Figure 4. Schematic presentation of the Au-ZnO-based nanocomposite thin films, their normalized visible absorption (a) and the surface plasmon resonance (SPR) (b) as influenced by the particle size/density (1) and the composition of the oxide matrix (2). The size/density of Au nanoparticles were adjusted by the time in which the metallic phase was grown (t_{metal}), whereas the composition of the oxide matrix was controlled by adjusting the composition of the liquid feedstock used in the CVD process.

$$\lambda_{max}^2 = \frac{\pi c^2 m_e(\varepsilon_0 + 2n^2)}{e^2 N_e} \quad (1)$$

Figure 4 (2a) shows the variation of the normalized visible absorption spectra of the films obtained with varied composition of the feedstock of the oxide phase, while t_{oxide} was kept constant at 20 min. The SPR, Figure 4 (2b), shows a linear increase with the fraction of titanium precursor in the CVD feedstock of the oxide phase. This linear dependency is in line with the calculated and experimental results reported by Cao et al.[25] and Medda et al.[10]

The proposed approach in this study exhibits an enormous potential for the synthesis of immobilized M1 nanoparticles of reactive and noble transition metals within the bulk of M2 functional oxide thin films. An accurate control of the nanoparticle size and of the composition of the nanoparticles and the host matrix was demonstrated. This highly flexible synthesis approach enables the rational design of metal–metal-oxide nanocomposite thin films and paves the way towards the development of multifunctional magnetic-optical and electrical devices, by using CVD which is a standard industrial micro-fabrication technique.

Received: April 11, 2011
Revised: June 6, 2011
Published online: September 9, 2011

Keywords: chemical vapor deposition (CVD) · magnetic nanocomposites · metal nanoparticles · nanocomposites · plasmon resonance

[1] A. Kafizas, S. Kellici, J. A. Darr, I. P. Parkin, *J. Photochem. Photobiol. A* **2009**, *204*, 183 – 190.
[2] K. Awazu, M. Fujimaki, C. Rockstuhl, J. Tominaga, H. Murakami, Y. Ohki, N. Yoshida, T. Watanabe, *J. Am. Chem. Soc.* **2008**, *130*, 1676 – 1680.
[3] T. Hirakawa, P. V. Kamat, *J. Am. Chem. Soc.* **2005**, *127*, 3928 – 3934.
[4] E. Thimsen, F. Le Formal, M. Grätzel, S. C. Warren, *Nano Lett.* **2011**, *11*, 35 – 43.
[5] a) M. K. Kwon, J. Y. Kim, B. H. Kim, I. K. Park, C. Y. Cho, C. C. Byeon, S. J. Park, *Adv. Mater.* **2008**, *20*, 1253 – 1257; b) W. H. Ni, J. An, C. W. Lai, H. C. Ong, J. B. Xu, *J. Appl. Phys.* **2006**, *100*, 026103.
[6] K. Okamoto, I. Niki, A. Shvartser, Y. Narukawa, T. Mukai, A. Scherer, *Nat. Mater.* **2004**, *3*, 601 – 605.
[7] T. J. Zhou, M. H. Lu, Z. H. Zhang, H. Gong, W. S. Chin, B. Liu, *Adv. Mater.* **2010**, *22*, 403 – 406.
[8] Y. Wang, J. Hu, Y. Lin, C.-W. Nan, *NPG Asia Mater.* **2010**, *2*, 61 – 68.
[9] G. Walters, I. P. Parkin, *J. Mater. Chem.* **2009**, *19*, 574 – 590.
[10] S. K. Medda, S. De, G. De, *J. Mater. Chem.* **2005**, *15*, 3278 – 3284.
[11] M. Es-Souni, S. Habouti, N. Pfeiffer, A. Lahmar, M. Dietze, C. H. Solterbeck, *Adv. Funct. Mater.* **2010**, *20*, 377 – 385.
[12] a) R. Serna, A. Suarez-Garcia, C. N. Afonso, D. Babonneau, *Nanotechnology* **2006**, *17*, 4588 – 4593; b) Z. Konstantinović, M. G. del Muro, M. Varela, X. Batlle, A. Labarta, *Nanotechnology* **2006**, *17*, 4106 – 4111.
[13] R. G. Palgrave, I. P. Parkin, *Chem. Mater.* **2007**, *19*, 4639 – 4647.
[14] a) R. G. Palgrave, I. P. Parkin, *J. Am. Chem. Soc.* **2006**, *128*, 1587 – 1597; b) A. Salaün, J. A. Hamilton, D. Iacopino, S. B. Newcomb, M. G. Nolan, S. C. Padmanabhan, I. M. Povey, M. Salaun, M. E. Pemble, *Thin Solid Films* **2010**, *518*, 6921 – 6926.
[15] N. Bahlawane, P. A. Premkumar, Z. Y. Tian, X. Hong, F. Qi, K. Kohse-Hoinghaus, *Chem. Mater.* **2010**, *22*, 92 – 100.
[16] P. A. Premkumar, N. S. Prakash, F. Gaillard, N. Bahlawane, *Mater. Chem. Phys.* **2011**, *125*, 757 – 762.
[17] N. Bahlawane, P. A. Premkumar, K. Onwuka, G. Reiss, K. Kohse-Hoinghaus, *Microelectron. Eng.* **2007**, *84*, 2481 – 2485.
[18] a) G. Mie, *Ann. Phys.* **1908**, *330*, 377 – 445; b) S. Link, M. A. El-Sayed, *J. Phys. Chem. B* **1999**, *103*, 4212 – 4217.
[19] H. A. Atwater, A. Polman, *Nat. Mater.* **2010**, *9*, 205 – 213.
[20] S. Palomba, L. Novotny, R. E. Palmer, *Opt. Commun.* **2008**, *281*, 480 – 483.
[21] P. K. Jain, W. Y. Huang, M. A. El-Sayed, *Nano Lett.* **2007**, *7*, 2080 – 2088.
[22] M. Losurdo, M. M. Giangregorio, G. V. Bianco, A. A. Suvorova, C. Kong, S. Rubanov, P. Capezzuto, J. Humlicek, G. Bruno, *Phys. Rev. B* **2010**, *82*, 155451.
[23] T. C. Prathna, N. Chandrasekaran, A. M. Raichur, A. Mukherjee, *Colloids Surf. B* **2011**, *82*, 152 – 159.
[24] G. Krylova, A. Eremenko, N. Smirnova, S. Eustis, *Int. J. Photoenergy* **2005**, *7*, 193 – 198.
[25] M. Cao, M. Wang, N. Gu, *J. Phys. Chem. C* **2009**, *113*, 1217 – 1221.

